

A Review of Synthesis, Electrochromic Polymerization, and Characterization of 4-Substituted Phenyl Containing Poly(dithienylpyrrole)s

Pei-Ying Lee ^{1*}, Tzi-Yi Wu ²

ABSTRACT

Conducting polymers (CPs) exhibit some significant properties such as flexibility, processability, and inherent conductivity due to overlap bands gap between the conduction and valence bands. π -conjugated polymers provide high electron affinity and low energy of optical or electrical transmission because of the width of the energy gap between the lower conduction band and the higher valence band. Organic electrochromic (EC) materials have a lot of benefits, for example, facile synthesis via chemistry and electrochromism, low oxidation voltage, high stability for long turn cycling, great optical contrast, fast response time, huge coloration efficiency, and multiple optical chromaticities. The polymer structure of phenyl dithiophenyl-pyrrole backbone has π -conjugated line lead to electrons delocalized transformation from one state to other orbitals, therefore increasing the conductivity of materials. This mini-review summary a series of 4-substituted phenyl-2,5-dithienylpyrrole derivatives, namely 1-(4-(methylthio)phenyl)-2,5-di(thiophen-2-yl)-pyrrole (MPS), 1-(4-methoxyphenyl)-2,5-di(thiophen-2-yl)-pyrrole (MPO), and 4-(2,5-di(thiophen-2-yl)-pyrrol-1-yl)benzotrile (ANIL), 2,5-di(thiophen-2-yl)-1-(4-(trifluoromethoxy) phenyl) pyrrole (TTPP), 2,5-di(thiophen-2-yl)-1-(4-(thiophen-2-yl)phenyl)-pyrrole (DTTPP), and 1-(4-(furan-2-yl)phenyl)-2,5-di(thiophen-2-yl)-pyrrole (FPT), were synthesized by using Paal-Knorr reactions and their homopolymers (PMPS, PMPO, PANIL, PTPP, PDTTPP, and PFPT) were integrated from electrochemical polymerizations. Their optical and electrochemical properties were introduced such as optical contrast, coloration efficiency, stability, and optical memory.

Keywords: conducting polymers; π -conjugated polymers; organic electrochromic materials; electrochemical polymerizations; optical contrast; coloration efficiency

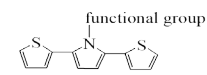
1. INTRODUCTION

Electrochromic materials can transform their spectroelectrochemical properties by undergoing electron-transfer process. They have a wide range of applications, including organic and inorganic materials such as automotive anti-glare rearview mirrors, energy-saving smart windows that adjust indoor light sources, safety helmet wind mirrors, aircraft portholes, electrochromic paper, automotive windows, skylights, etc. (Zhili et al. 2020). Compared to inorganic electrochromic materials, organic ones have many advantages such as simple synthesis and processability, low cost for final products, a large number of colors for polymeric materials, and favorable optical properties (Zhili et al. 2020).

Recently, CPs polymers had major attention in academic and industrial applications, because those polymers reserved high conductivity and stability of initial monomers (Camurlu et al. 2020). In the past two decades, polypyrroles (PPys) and polythiophenes (PThs) were abroad manufactured and applications. However, thiophenes restrained their utilizations including low solubili-

ty and high deposition potential of those final polymers. Widespread research contributed to improving their properties through functionalizations of organic synthesis. Nevertheless, insertion of functional groups into PPys or PThs produced lower conductivity as a result of steric hindrances induced decreasing the length of conjugation (Camurlu et al. 2020).

The chemical structures consist of p -conjugated backbones that permit low energy of electric transmission to induce higher conductivity. Owing to the different deposition potentials between pyrrole ($E_{OX} = 1.1V$) and thiophene ($E_{OX} = 1.8V$), the best choice is to synthesize hybrid monomeric structures comprising thiophene and pyrrole rings, namely 2,5-di(thienyl)pyrroles (SNSs) shown in Figure 1 (Camurlu et al. 2020).



N -substituted-2,5-di(thienyl)pyrrole derivatives

SXS
X = NH, NMe, O, S

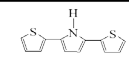
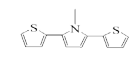
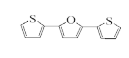
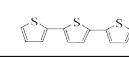
Chemical structure	Full name	Abbreviation
	2,5-di(thiophen-2-yl)pyrrole	SNS when X = NH
	<i>N</i> -methyl-2,5-di(thiophen-2-yl)pyrrole	SMS when X = NMe
	2,5-di(thiophen-2-yl)furan	SOS when X = O
	2-(5-(thiophen-2-yl)thiophen-2-yl)thiophene	SSS when X = S

Fig. 1 The structure of *N*-substituted-2,5-di(thienyl)pyrrole derivatives

Manuscript received March 2, 2022; revised March 29, 2022; accepted May 16, 2022.

^{1*} Postdoctoral Researcher, Department of Chemical and Materials Engineering, National Yunlin University of Science and Technology, Taiwan R.O.C.
(email: leepy@yuntech.edu.tw)

² Professor, Department of Chemical and Materials Engineering, National Yunlin University of Science and Technology, Taiwan R.O.C.

In 1989, Ferraris et al. introduced different functional groups between two thiophenes, namely SNS (2,5-di(thiophen-2-yl)pyrrole), SMS (N-methyl-[2,5-di(thiophen-2-yl)]pyrrole), SOS (2,5-di(thiophen-2-yl)furan), SSS (2-(5-(thiophen-2-yl)thiophen-2-yl)thiophene). The SNS structure has lower oxidation potential and longer conjugation than the SSS structure, which indicated electrons can be transferred better, resulting in larger polaron and bipolaron. However, SMS with methyl substituents on SNS pyrrole has the same electrochemical characteristics as SNS, and the substituent groups on SMS can prevent producing unstable quinoid structures. Because the quinoid phase makes the SMS polymer film more resistant to falling off than SNS one (Ferraris et al. 1989). All of the above reasons imply that SNS can be more chemically modified through Paal-Knorr reaction.

In 2006, Tarkuc, S and Toppare, L. et al attached 1,4-di(thiophene-2-yl) butane- 1,4-dione to aniline group, named it PTP, and its initial potential 0.45 V measured by cyclic voltammetry. In the UV-VIS absorption spectrum, it can be found that there were absorption peaks of $\pi-\pi^*$ at 413 nm, polaron and bipolaron peaks gradually formed at 577 nm and 884 nm, and its optical contrast value was 27% at 413 nm by different voltages (Tarkuc and Toppare et al. 2006). In the next year, Yigitsoy, B. and Toppare, L. et al. functionalized a 4-methylbenzene ring on the pyrrole in the center of the SNS structure through the Paal-Knorr reaction, and exposed that it has obvious and reversible redox peaks at 0.43V and 0.30V, respectively. In the spectroelectrochemical spectrum, the maximum absorbance wavelength presented a $\pi-\pi^*$ transition at 428 nm for the homopolymer, polaron and bipolaron bands formation at 620 nm and 1000 nm, respectively. Furthermore, it has 29% of the optical contrast value, and about 1.5 seconds of the conversion time. Therefore, the material has good stability from the graph of penetration vs. time (Yigitsoy and Toppare et al. 2007). In the same year, Arslan, Adu and Toppare, L. et al. successfully chemical synthesized 1-(4-Fluorophenyl)-2,5-di(thiophen-2-yl)-1H-pyrrole (FPTP) and electro-chemically polymerized to produce its polymer. Optoelectrochemistry was investigated that $\pi-\pi^*$ transition of P(FPTP) was observed at 398 nm, polaron and bipolaron bands formations occurred at 510 nm and 850 nm, respectively. Switching time and optical contrast were found as 1.4 s and 19.4% at maximum contrast point, respectively (Arslan and Toppare et al. 2007).

In 2010, Shim et al. chemically modified the 4-benzonitrile group on the pyrrole in the center of the SNS construction via the Paal-Knorr reaction and successfully synthesized the DPB (2,5-di(2-thienyl)-1H-pyrrole-1-(p-benzoic acid) structure through base-catalyzed hydrolysis nitriles reactions. According to the cyclic voltammetry diagram, the DPB has about 0.7 V of the starting potential and different scanning speeds indicated that the film has the characteristics of layer upon layer. The color is yellow at 0 V, and blue at 1.0 V, with a transmittance difference of about 30%, and it still maintains good stability after 700 cycles of back and forth (Shim. et al. 2010).

In 2014, Eken, S. et al introduced a halogen group on the benzene ring of the SNS side chain. Taking the Br group as an example, the meta and para positions on the benzene ring were named *m*-BrPTP and *p*-BrPTP, and their starting potentials were 0.85 V and 0.78 V, respectively (Eken et al. 2014). Comparing with the PTP structure published by Tarkuc, S. et al, the starting potentials were significant increases, because halogens were the electron withdrawing groups, which caused the initial potentials to become higher. In the UV-VIS absorption spectrum, it can be found that absorption peaks of $\pi-\pi^*$ from P(*m*-BrPTP) and P(*p*-BrPTP) were at 417 nm and 407 nm, respectively. As the potential rises, the $\pi-\pi^*$ absorption peaks of P(*m*-BrPTP) and P(*p*-BrPTP)

gradually becomes smaller, and new absorption peaks are generated at 514 nm and 576 nm, respectively. Therefore, it can be seen that introduced different groups and position in the side chain of SNS structures would change their electrochemical and optical properties (Yildiz and Tarkuc et al. 2006).

Published articles by Yigitsoy, B. and Toppare, L. et al in 2007 and Yildiz, E and Toppare et al. in 2008 indicated not only changing the structure of the functional groups on the pyrrole of a series of SNS polymers, but also polymerizing a series of SNS monomers with various other ones into copolymers. Those operations can improve their electrochromic properties and induce the color to become more colorfully (Yigitsoy and Toppare et al. 2007), (Yildiz and Toppare et al. 2008). In the literature published by Prof. Amb, C. M. in 2011, discovered that not only the electron influence but also the steric effect of functional groups of polymers could impact the color change and affected their conjugation. And the extent of redshifts that the position of absorption peaks of polymers leads to achieving the effect of color fine-tuning (Amb et al. 2011). In the literature published by Akbaşoğlu, N. and Toppare, L. et al in 2010, they revealed the addition of di-thiophene and furan to electrochromic materials would affect the initial oxidation potential of the cyclic voltammetry and also cause the redshift phenomenon on spectroelectrochemical properties (Akbaşoğlu et al. 2010).

In 2002, Prof. Gaupp, C. L. and et al published ProDOT-Et₂ on a document. They exposed a maximum absorption peak at 580 nm on the UV-VIS spectrum and its optical contrast value reached 75%, and it has high optical stability (Gaupp et al. 2002). In 2010, Prof. Huang, J. H. and other scholars published a document comparing the optical properties of cathode materials of PXDOTs derivatives, including EDOT, ProDOT, ProDOT-Me₂, and ProDOT-Et₂. From the results, ProDOT-Et₂ has the highest value of optical contrast, the lowest conversion time, and the most outstanding coloring efficiency. It is a very good material of electrochromic cathodes (Huang et al. 2010). Table 1. described optical properties of PXDOTs materials of electrochromic cathode, including the greatest wavelengths of absorption peak, optical contrast values, conversion times, and coloring efficiencies (Huang et al. 2010).

Table 1 Optical properties of PXDOTs electrochromic cathode materials (Huang et al. 2010)

Polymer	Chemical structure	λ_{max} (nm)	Contrast $\Delta T(\%)$	Switching time τ (s)	Coloring efficiency η (cm ² C ⁻¹)
PEDOT		600	53	2.8	250
PProDOT		560	66	1.2	393
PProDOT-Me ₂		580, 630	70	2.3	580
PProDOT-Et ₂		580, 632	74	0.9	760

In 2001, Prof. Krishnamoorthy, K. and other researchers successfully synthesized the cathode material ProDOT-Bz₂ introducing two benzene rings which made the structure more regular and symmetrical. Therefore, increasing the separation between chains leads to achieving better optical contrast. From the UV-VIS absorption spectrum, they indicated the largest absorption peak at 632 nm. At this wavelength, the optical contrast value reached

89%, and the coloring efficiency reached $575 \text{ cm}^2 \text{ C}^{-1}$ (Krishnamoorthy et al. 2001). In 2012, Prof. İçli-Özkut, M. and other scholars published an article of comparison of five cathode materials. They demonstrated that ProDOT-Bz2 has better optical contrast and coloring efficiency near 630 nm than other similar structures (İçli-Özkut et al. 2012). In 2016, Prof. Kuo, C. W. and other scholars published an article. They discovered a phenomenon when they measured the optical properties of the anode material P(BCz-co-Inc) and the cathode material PProDOT-Et2, the UV-VIS spectrum procured an absorption peak at 587 nm as voltages raising. The maximum absorption peak has an optical contrast value of 42%, the coloring efficiency reaches $634 \text{ cm}^2/\text{C}$, and the color changes from -1.3 V colorless transparent to 1.3 V blue-black. From comparison results of the above cathode materials, ProDOT-Bz2 and ProDOT-Et2 have superior optical properties (Kuo et al. 2016). Table 2. compared the optical properties of cathode material derivatives including ProDOS and ProDOT.

Table 2 Comparison optical properties of ProDOS and ProDOT cathode material derivatives. (İçli-Özkut et al. 2012)

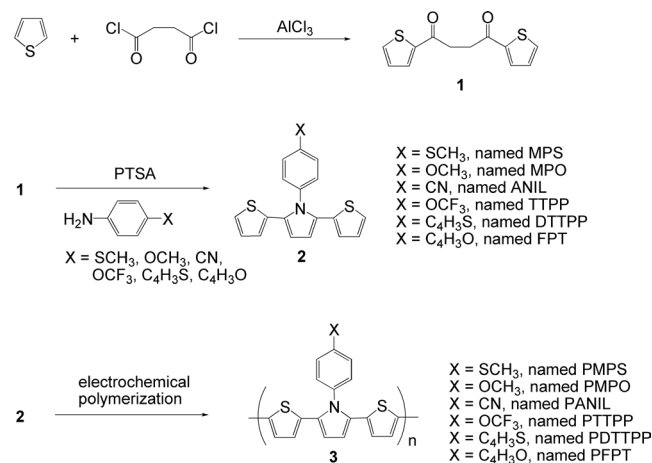
Polymers					
$E_{\text{onset}}^{\text{red}}$ (V)	1.37	1.42	1.40	1.55	1.39
$E_{\text{p}1/2}^{\text{ox}}$ (V)	0.28	0.41	0.14	0.35	0.35
Stability (After 5000 switching)	89	67	63	68	97
$\Delta\%T$	67% at 645 nm	75% at 630 nm	64% at 630 nm	73% at 622 nm	56% at 636 nm
CE(cm^2/C)	992	551	337	306	328
E_g	1.62	1.86	1.85	1.82	1.58
λ_{max}	645, 710	575, 630	559, 630	571, 622	636, 697

Therefore, this study concentrated on these two cathode materials and a series of synthesized anode materials that were forming a complementary element and testing its electrochemical and optical properties. Among them, the color change of the physical state and the oxidation state, whether the color change of the anode material or the cathode material, which is not only affected by electrons, but also by the basic structure of the functional groups.

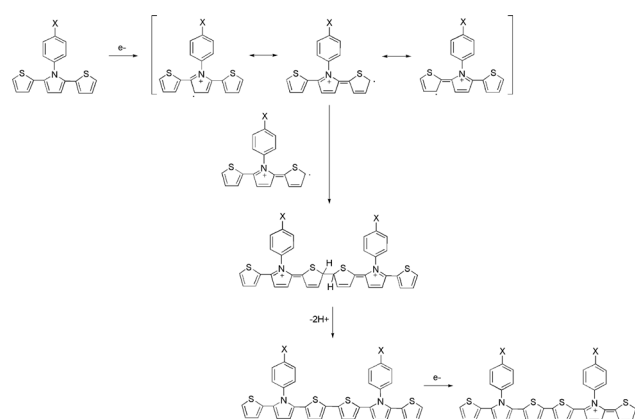
2. MATERIALS AND METHODS

In this review article, we focus on synthesis of 4-substituted phenyl SNS derivatives, such as MPS, MPO, ANIL, TTPP, DTTTP, and FPT (Su and Wu et al. 2017; Wang and Wu et al. 2020; Wu and Tung et al. 2018; Wang, Chang, and Wu et al. 2019). These 4-substituted phenyl groups functionalized SNS monomers were prepared from 1,4-di(2-thienyl)-1,4-butanedione and 4-substituted aniline groups as starting reagents through Paal-Knorr condensation reactions. A series of confirmations have been confirmed that coplanarity produced effective conjugation and inter-moleculars retained electric conductivity, charge transmission, and purposed functionalization. The electrochemical polymerization of dithienylpyrrole hybrid backbones possesses low oxidation potentials and excellent stability of oxidation states to resulting polymers. The synthetic techniques of 4-substituted phenyl groups functionalized SNS monomers and polymers were illustrated in Scheme 1. As a result of reducing band gaps and advanced stability of terminated polymers, improving conductivity and conducting

moieties for final products. The electrochemical deposition mechanism of the phenyl-SNS backbone is represented in Scheme 2. The phenyl-SNS monomer obtained the electron to form the phenyl-[SN⁺S] structure which has three resonance ones. After that, respectively two free radicals on two phenyl-SNS monomers generated one carbon-carbon bond and released two hydrogen atoms. Therefore, the length of phenyl-SNS conjugated backbone was increased through these two steps repeatedly.



Scheme 1 Synthetic routes of 4-substituted phenyl groups functionalized SNS monomers and polymers (Su and Wu et al. 2017; Wang and Wu et al. 2020; Wu and Tung et al. 2018; Wang, Chang, and Wu et al. 2019).



Scheme 2 The mechanism of electrochemical polymerization for 4-substituted phenyl groups functionalized SNS monomers

Organic electrochromic devices demonstrate reversibly optical properties including absorbance, transmittance, and colors transformation by the application of a voltage. Generally, EC materials are coated over ITO glasses as thin films and placed in conducting glass substrates as an electrochemical cell. Subsequently, it can be filled up with suitable electrolytes to form the device. EC devices are composed of transparent indium tin oxide (ITO) conducting oxide glasses, suitable electrolyte layers, counter electrode layers and EC materials. The actual construction of the EC device was shown in Figure 2. Their structures are similar to sandwich multi-layer constitutions, which endure electrochemical oxidation-reduction reactions under an external electric field, that prompt reversibly multiple colorations in distinct optical states.

Organic conductive polymers are also called conjugated

polymers which are formed by alternately conjugated bonding of single and double bonds. π electrons easy delivery in the chain and make materials have conductive characteristics. Although π electrons are easy to move in the chain and they are also quite localized, they cannot obtain good conductivity. Therefore, it is necessary to doping which means to remove or inject some electrons from the chain. So that these holes or extra electrons can transfer on the molecular chain, and lead to the polymer becoming a conductor and increasing its conductivity. The energy gap of conductive polymers has similar to semiconductors. The energy gap is smaller and electrons of molecules is easier to be excited. HOMO and LUMO refer to the highest occupied molecular orbital and the lowest unoccupied molecular orbital, respectively. In organic semiconductors, HOMO is similar to the valence band of inorganic semiconductors and LUMO is similar to the conduction band of inorganic semiconductors. When the conductive polymer undergoes oxidative doping, π electrons are transferred from the π bond to form free radicals and cations, namely polarons. When further oxidized doping, the polarons increase continuously and form double cations, namely bipolarons. Bipolarons can change energy levels between valence bands and conduction ones. Electronic transitions required these energy changes, and they also change optical properties and produce different colors. Scheme 3 displays the mechanism of the color change for conjugative SNS polymers. Therefore, EC materials display various colorations owing to oxidation and reduction processes causing electrons delivery across different states in the effect of the electric field.

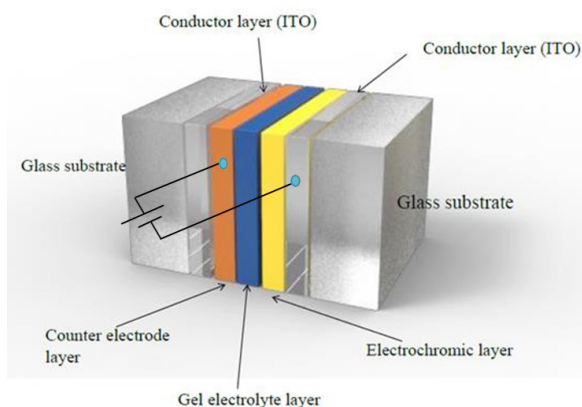
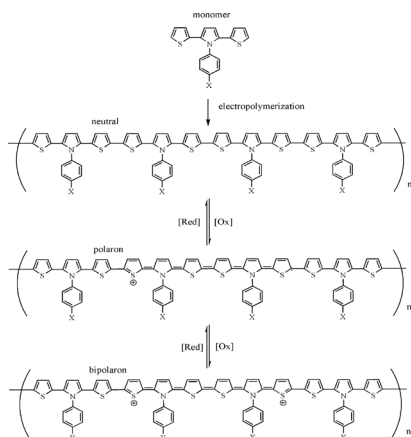


Fig 2 The schematic of the electrochromic device



Scheme 3 The mechanism of the color change for conjugative SNS polymers

3. RESULTS AND DISCUSS

3.1 Electrochemical Polymerizations of Anodic Monomers Using Cyclic Voltammetry

This section will discuss a series of successfully synthesized SNS monomers of anode materials (MPS, MPO, ANIL, TTPP, DTTTP, and FPT) for property testing. First, we use a potentiostat (CHI) (CH Instruments, Electrochemical analyzer, Electrochemical workstation) to find the starting potential of each material by cyclic voltammetry. After that, the monomer is polymerized on the ITO glass to form a film by the constant potential polymerization method, and then the optical properties are measured with a UV-Vis spectrometer.

We use a potentiostat (CHI) (CH Instruments, Electrochemical analyzer, Electrochemical workstation) for cyclic voltammetry test to find the initial oxidation potential in the first circle. The electrochemical system uses a three-electrode system, including the LiClO_4 auxiliary electrolyte solution, 2 mM the monomer concentration, ITO glass as the working electrode, platinum wire as the auxiliary electrode, Ag/AgCl (sat KCl) as the reference electrode, scanning voltage from -1 to 1.4 V, scanning rate is 100 mV/sec, and scanning twenty circles.

From the cyclic voltammogram, the initial potential of each material is in the first circle. After scanning 20 circles, it can be found the number of scan circles increases, and the current density of the redox peak also increases. The first loop is the first layer that is polymerized on the ITO glass. If the second layer is to be polymerized, the current density will need to increase to be stacked on the first layer. Therefore, the current density increases with the number of turns. It means that the conductive polymer film is stacked on the ITO glass layer by layer.

Figure 3 shows the cyclic voltammograms of electrochemical polymerization. The beginning potentials of MPS, MPO, ANIL, TTPP, DTTTP, and FPT are 0.7, 0.69, 0.81, 0.68, 0.68, and 0.74 V, respectively. The basis potential of MPS is approximate to MPO, indicating the methylthio-phenyl or methoxyphenyl section shows a similar electron-donating characteristic. However, the benzonitrile part shows a larger opening potential than those units, representing including electron-withdrawing groups on the nitrogen atom of the pyrrole ring which increases the inception potential significantly. The oxidation and reduction peaks of PMPS, PMPO, PANIL, PTTTP, PDTTTP, and PFPT are located at 0.95 V; 0.5 V, 0.9 V; 0.55 V, 1.0 V; 0.6 V, 0.77 V; 0.17 V, 0.94 V; 0.47 V, and 0.74 V; 0.57 V, respectively (Su and Wu et al. 2017; Wang and Wu et al. 2020; Wu and Tung et al. 2018; Wang, Chang, and Wu et al. 2019).

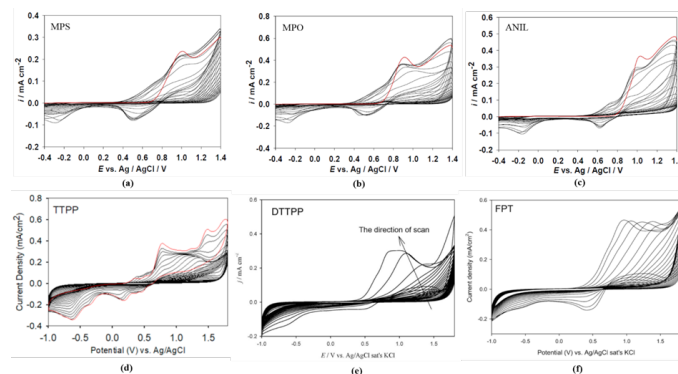


Fig. 3 Cyclic voltammograms of (a) MPS, (b) MPO, (c) ANIL, (d) MPS, (e) MPO, and (f) ANIL in ionic solutions. The red line indicates the first cycle of CVs (Su and Wu et al. 2017;

Wang and Wu et al. 2020; Wu and Tung et al. 2018; Wang, Chang, and Wu et al. 2019).

Figure 4a–f shows the redox relationship between the peak current and scan rate of PMPS, PMPO, PANIL, TTPP, DTTTP, and FTP films in an ionic solution at different scanning rates (Su and Wu et al. 2017; Wang and Wu et al. 2020; Wu and Tung et al. 2018; Wang, Chang, and Wu et al. 2019). Figure 4g–l describes a linear among the scan rate and redox current densities and indicates the redox processes are not diffusion controlled. And the electroactive polymer films are well-adhered on the ITO-coated electrode surface (Su and Wu et al. 2017; Wang and Wu et al. 2020; Wu and Tung et al. 2018; Wang, Chang, and Wu et al. 2019).

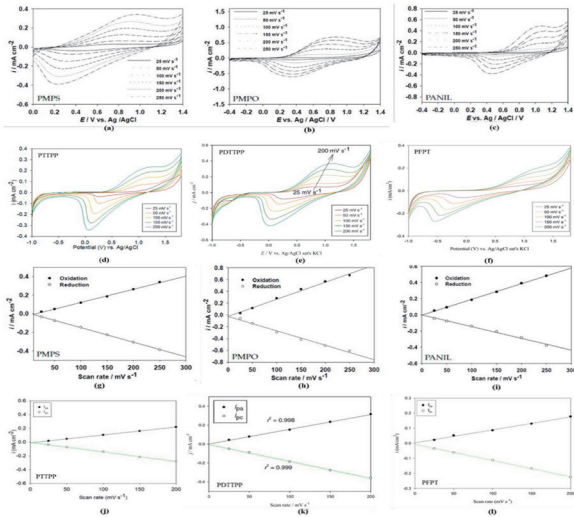


Fig. 4 Cyclic voltammograms of (a) PMPS, (b) PMPO, (c) PANIL, (d) PTTTP, (e) DTTTP, and (f) PFPT films between 25 and 250 mV/s-1 scan rates in ionic solutions. The linear relationship between the peak current density and scan rate of (g) PMPS, (h) PMPO, (i) PANIL, (j) PTTTP, (k) DTTTP, and (l) PFPT films in ionic solution (Su and Wu et al. 2017; Wang and Wu et al. 2020; Wu and Tung et al. 2018; Wang, Chang, and Wu et al. 2019).

3.2 Electrochromic Characteristic of Polymer Films

Figure 5a–f shows the UV/VIS spectra of (a) PMPS, (b) PMPO, (c) PANIL, (d) PTTTP, (e) DTTTP, and (f) PFPT films. The PMPO film shows an obvious $\pi-\pi^*$ transition peak at about 421 nm, in spite of the PMPS film showing a shoulder at about 440 nm in the UV/VIS spectra, implying the including of a methylthio group in the polymer backbone leads to redshift in the absorption band. However, the applying of an electron-withdrawing benzonitrile part into the 4-substituted phenyl-SNS backbone deactivates, named PANIL, the $\pi-\pi^*$ transition blueshift to 360 nm. When the potentials increase above +0.8 V (vs. Ag/AgCl), the shoulder of the PMPS film at around 440 nm and the absorption peak of the PANIL film at around 360 nm decrease progressively, and the charge carrier bands appear at about 600–1000 nm (Su and Wu et al. 2017; Wang and Wu et al. 2020; Wu and Tung et al. 2018; Wang, Chang, and Wu et al. 2019). The $\pi-\pi^*$ transition peak of PTTTP film in the reduction state is situated at 364 nm in the UV/Vis band. However, absorption peaks of PDTTPP and PFPT films in a neutral state were located at 439 and 407 nm. This blueshift phenomenon of the $\pi-\pi^*$ transition is generated from decorating the electron-withdrawing trifluoromethoxy group into para-sub-

stituted phenyl-dithienopyrrole backbone derivatives. Upon applying sufficiently high voltages to PTTTP, PDTTPP, and PFPT films, the absorbance of their $\pi-\pi^*$ transition peak started to decrease and polaron/bipolaron bands emerged at around 532/1050 nm, 572/970 nm, and 590/1320 nm (Su and Wu et al. 2017; Wang and Wu et al. 2020; Wu and Tung et al. 2018; Wang, Chang, and Wu et al. 2019).

Figure 4a–f shows the redox relationship between the peak current and scan rate of PMPS, PMPO, PANIL, TTPP, DTTTP, and FTP films in an ionic solution at different scanning rates (Su and Wu et al. 2017; Wang and Wu et al. 2020; Wu and Tung et al. 2018; Wang, Chang, and Wu et al. 2019). Figure 4g–l describes a linear among the scan rate and redox current densities and indicates the redox processes are not diffusion controlled. And the electroactive polymer films are well-adhered on the ITO-coated electrode surface (Su and Wu et al. 2017; Wang and Wu et al. 2020; Wu and Tung et al. 2018; Wang, Chang, and Wu et al. 2019).

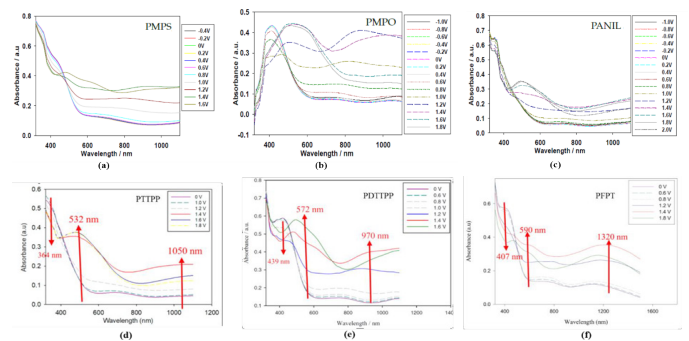


Fig. 5 Spectroelectrochemical spectra of (a) PMPS, (b) PMPO, (c) PANIL, (d) PTTTP, (e) DTTTP, and (f) PFPT films coated on an ITO glass electrode at different potentials in ionic solutions (Su and Wu et al. 2017; Wang and Wu et al. 2020; Wu and Tung et al. 2018; Wang, Chang, and Wu et al. 2019).

Table 3 shows the photos of PMPS, PMPO, and PANIL in the ionic solution at 0V and +1.6V potentials. The PMPS film was green, and the PMPO and PANIL films were light green at 0 V in the neutral state. However, the PMPS film was brown, and the PMPO and PANIL films were blue and grey at 1.6V in the highly oxidized state, respectively. Table 4 shows the photos of PTTTP, PDTTPP, and PFPT in the ionic solution at 0V and +1.4V potentials. The PTTTP, PDTTPP, and PFPT films were grayish-yellow, yellowish green, and saffron yellow at 0 V in the neutral state. The PTTTP, PDTTPP, and PFPT films were grayish-blue, bluish purple, and yellowish-gray at 1.0 V in the oxidized state. The PDTTPP and PFPT films were bluish purple and light purple at 1.2 V in the oxidized state. The PTTTP, PDTTPP, and PFPT films were bluish-violet, deep bluish violet, and bluish-purple at 1.4 V in the highly oxidized state. The incorporation of the MPS, TTPP, or DTTTP units into the PSNS backbone gives to darker color than those of the MPO, ANIL, FPT units (Su and Wu et al. 2017; Wang and Wu et al. 2020; Wu and Tung et al. 2018; Wang, Chang, and Wu et al. 2019).

Table 3 Electrochromic behaviors of PMPS, PMPO, PANIL, and their EDCs in the ionic solution at 0V and +1.6V potentials (Su and Wu et al. 2017).

Polymer Films and ECDs	Reduction (0 V)	Oxidation (+1.6 V)
PMPS		
PMPO		
PANIL		
PMPS/PProDOT-Et ₂		
PMPO/PProDOT-Et ₂		
PANIL/PProDOT-Et ₂		

Table 4 Electrochromic behaviors of TTPP, DTTPP, and FTP films (Wang and Wu et al. 2020; Wu and Tung et al. 2018; Wang, Chang, and Wu et al. 2019).

Polymers	E/V	Photographs	L*	a*	b*
PTTPP	0		92.11	-2.13	19.48
	1.0		91.09	-2.13	17.43
	1.4		75.4	6.8	4.77
PDTTPP	0		82.0	1.67	35.1
	1.0		81.3	0.90	32.4
	1.2		74.3	1.83	14.6
	1.4		65.7	3.68	3.92
	1.6		64.25	1.41	3.69
PFPT	0		82.51	1.63	33.23
	1.0		80.68	-1.07	24.1
	1.2		77.66	-1.28	15.7
	1.4		74.24	-0.72	9.29
	1.6		70.62	3.46	1.04

L* indicates the lightness, a* and b* represent the color channels.

Figure 6. shows the CIE (Commission Internationale de l'Eclairage) chromaticity diagrams of the PMPS, PMPO, PANIL, PTTPP, DTTPP, and PFPT films in neutral and oxidation states, and the colorimetric values (L, a, b, L*, a*, and b*) and CIE chromaticity values (x, y) of the three polymer films at various potentials in the ionic solution are summarized in Table 3, Table 4, and Table 5 (Su and Wu et al. 2017; Wang and Wu et al. 2020; Wu and Tung et al. 2018; Wang, Chang, and Wu et al. 2019).

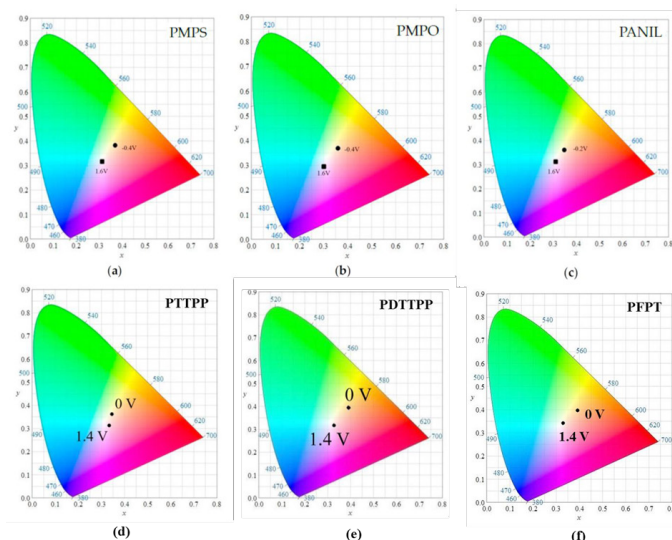


Fig. 6 The CIE chromaticity diagrams of (a) PMPS, (b) PMPO, (c) PANIL, (d) PTTPP, (e) DTTPP, and (f) PFPT films in neutral and oxidation states (Su and Wu et al. 2017; Wang and Wu et al. 2020; Wu and Tung et al. 2018; Wang, Chang, and Wu et al. 2019)

Table 5 Electrochromic behaviors of TMPS, PMPO, and PANIL films (Su and Wu et al. 2017).

Polymers	E/V	L	a	b	L*	a*	b*	x	y
PMPS	-0.4	80.25	-1.00	25.76	84.17	0.09	31.17	0.3726	0.3828
	-0.2	80.24	-0.92	25.75	84.17	0.17	31.16	0.3727	0.3827
	0	80.37	-1.16	25.83	84.27	-0.08	31.25	0.3724	0.383
	0.2	80.26	-0.93	25.73	84.18	0.16	31.12	0.3726	0.3826
	0.4	80.32	-1.06	25.72	84.23	0.03	31.1	0.3723	0.3826
	0.6	80.19	-1.35	25.35	84.13	-0.28	30.55	0.3708	0.3819
	0.8	79.38	-1.78	23.81	83.45	-0.73	28.4	0.3663	0.3784
	1.0	76.51	-1.99	18.99	81.03	-1.01	21.93	0.3541	0.3666
	1.2	72.95	-1.61	13.51	78	-0.66	14.98	0.3413	0.3526
	1.4	67.69	-0.39	6.78	73.42	0.57	6.93	0.3269	0.3346
	1.6	64.25	1.41	3.69	70.37	2.52	3.40	0.3227	0.3251
PMPO	-0.4	84.19	0.76	24.26	87.42	1.91	28.09	0.3677	0.3731
	-0.2	84.19	0.74	24.29	87.42	1.9	28.13	0.3678	0.3732
	0	84.16	0.7	24.31	87.4	1.85	28.15	0.3677	0.3733
	0.2	84.16	0.56	24.23	87.4	1.71	28.04	0.3673	0.3733
	0.4	83.98	-0.05	23.49	87.25	1.1	27.01	0.3645	0.3719
	0.6	83.12	-0.97	21.06	86.55	0.15	23.77	0.3571	0.3667
	0.8	81	-1.31	16.05	84.8	-0.22	17.39	0.3447	0.3549
	1.0	75.3	-0.14	5.62	80.01	0.92	5.23	0.3228	0.3296
	1.2	67.81	2.85	-2.19	73.53	4.07	-3.2	0.31	0.3087
	1.4	61.26	3.77	-4.04	67.67	5.12	-5.21	0.3069	0.3024
	1.6	61.06	4.08	-3.24	67.49	5.46	-4.36	0.3095	0.3041
1.8	61.94	4.08	-2.58	68.29	5.45	-3.64	0.3113	0.306	
PANIL	-0.4	87.66	-0.42	20	90.25	0.76	21.69	0.3525	0.3606
	-0.2	87.71	-0.44	20.01	90.29	0.74	21.7	0.3525	0.3606
	0	87.74	-0.47	20.03	90.32	0.71	21.71	0.3525	0.3606
	0.2	87.79	-0.52	20.03	90.35	0.66	21.71	0.3524	0.3606
	0.4	87.78	-0.64	19.96	90.35	0.55	21.62	0.352	0.3606
	0.6	87.69	-0.93	19.58	90.28	0.25	21.13	0.3507	0.3599
	0.8	87.11	-1.29	18.28	89.81	-0.11	19.55	0.3473	0.3573
	1.0	85.34	-1.45	15.21	88.36	-0.3	15.9	0.3406	0.3508
	1.2	80.64	-0.96	8.74	84.5	0.13	8.55	0.3277	0.3365
	1.4	74.34	0.8	3.1	79.19	1.9	2.44	0.3185	0.3229
	1.6	70.62	3.46	1.04	75.99	4.7	0.25	0.3186	0.3161
1.8	69.85	5.35	1.53	75.32	6.69	0.81	0.3231	0.3158	
2.0	70.35	5.88	2.85	75.76	7.24	2.26	0.3272	0.3185	

The optical band gap (Eg) can be calculated according to the Planck equation (1), where λ is the wavelength at which the onset of absorption occurs (Tsao and Wu et al. 2011).

$$E_g = 1241/\lambda_{\text{onset}} \tag{1}$$

For example, the Eg of PMPS, PMPO, PANIL, PTTPP, PDTTPP, and PFPT were 2.25, 2.17, 2.21, 2.34, 2.24, and 2.26 eV, respectively. A lower Eg value owing to the lowest unoccupied molecular orbital (LUMO) and highest occupied molecular orbital (HOMO) energy levels which were determined by cyclic voltam-

metry. The PSNS backbone was decorated methoxyphenyl showed the lowest E_g than those of the methylthio-phenyl, benzonitrile, trifluoromethoxy-phenyl, furanyl-phenyl, and thiophenyl-phenyl groups (Su and Wu et al. 2017; Wang and Wu et al. 2020; Wu and Tung et al. 2018; Wang, Chang, and Wu et al. 2019).

The E_{HOMO} was calculated from E_{onset} using the equation (2), where E_{onset} is the onset potential of oxidation.

$$E_{HOMO} = -e(E_{onset} + 4.8 \text{ V}) \text{ (vs. vacuum)} \quad (2)$$

E_{LUMO} of the polymers was calculated using the formula (3) (Wu and Chen et al. 2002).

$$E_{LUMO} = E_{HOMO} + E_g \quad (3)$$

For instance, the HOMO energy level and the LUMO energy level of PMPS, PMPO, PANIL, PTTTP, PDTPP, and PFPT are -4.90 and -2.65; -4.88 and -2.71; -5.00 and -2.79; -4.91 and -2.57; -4.85 and -2.61; -4.97 and -2.71 eV, respectively. The PANIL film shows the lowest LUMO energy level than those of the PMPS, PMPO, PTTTP, PDTPP, and PFPT films, and this can be attributed to the incorporation of an electron withdrawing cyano group in the ANIL unit that decreases the LUMO energy level significantly (Su and Wu et al. 2017; Wang and Wu et al. 2020; Wu and Tung et al. 2018; Wang, Chang, and Wu et al. 2019).

A square-wave cyclic potential step method accompanied by UV-Vis spectroscopy was used to determine the optical contrast and switching time of the PMPS, PMPO, PANIL, PTTTP, PDTPP, and PFPT films. The polymer films were immersed in ionic solution and stepped by repeated potential between neutral and oxidation states with a time interval of 5 s. Figure 7 exhibits the transmittance-time profiles of the PMPS film at 600 and 940 nm, the PMPO film at 584 and 950 nm, the PANIL film at 566 and 950 nm, the PTTTP film at 532 and 1050 nm, the PDTPP film at 572 and 970 nm, and the PFPT film at 590 and 1320 nm (Su and Wu et al. 2017; Wang and Wu et al. 2020; Wu and Tung et al. 2018; Wang, Chang, and Wu et al. 2019).

Table 6, Table 7, Table 8, and Table 9 summarized the coloration switching time (τ_c) and bleaching switching time (τ_b) of the PMPS, PMPO, PANIL, PTTTP, PDTPP, and PFPT films in the ionic solution. The optical switching time ($T_{95\%}$) of the PMPS film is 2.21 and 1.97 s at 600 and 940 nm, respectively, from the bleaching state to the coloring state at the 100th cycle, and 1.93 and 2.01 s at 600 and 940 nm, respectively, from the coloring state to the bleaching state at the 100th cycle. The optical switching time ($T_{95\%}$) of the PMPO film is 1.92 and 1.87 s at 584 and 890 nm, respectively, from the bleaching state to the coloring state at the 100th cycle, and 1.76 and 2.01 s at 584 and 890 nm, respectively, from the coloring state to the bleaching state at the 100th cycle. The optical switching time ($T_{95\%}$) of the PANIL film is 2.01 and 2.08 s at 566 and 950 nm, respectively, from the bleaching state to the coloring state at the 100th cycle, and 2.08 and 2.14 s at 566 and 950 nm, respectively, from the coloring state to the bleaching state at the 100th cycle. The optical switching time ($T_{95\%}$) of the PTTTP film is 2.29 and 2.39 s at 532 and 1050 nm, respectively, from the bleaching state to the coloring state at the 100th cycle, and 2.07 and 1.95 s at 532 and 1050 nm, respectively, from the coloring state to the bleaching state at the 100th cycle. The optical switching time ($T_{95\%}$) of the PDTPP film is 1.60, 2.44 and 1.68 s at 409, 572, and 970 nm, respectively, from the bleaching state to the coloring state at the 100th cycle, and 1.47, 0.87 and 1.86 s at 409, 572, and 970 nm, respectively, from the coloring state to the bleaching state at the 100th cycle. The optical switching time ($T_{95\%}$) of

the PFPT film is 1.82 and 1.90 s at 590 and 1320 nm, respectively, from the bleaching state to the coloring state at the 100th cycle, and 2.03 and 1.91 s at 590 and 1320 nm respectively, from the coloring state to the bleaching state at the 100th cycle (Su and Wu et al. 2017; Wang and Wu et al. 2020; Wu and Tung et al. 2018; Wang, Chang, and Wu et al. 2019).

Table 6 Color-bleach kinetics of PMPS, PMPO, and PANIL films in ionic solutions and ECDs (Su and Wu et al. 2017).

Polymer Films and ECDs	λ_{max}/nm	Cycle No.	Optical Contrast/%		Optical Contrast/%	
			$\Delta T/\%$	$T_{95\%}$	$\Delta T/\%$	$T_{95\%}$
PMPS film in [EPI ⁺][TFSI ⁻]	600	1	17.59	2.22	17.59	2.01
		50	17.27	2.16	17.28	2.08
		100	18.62	2.21	18.61	1.93
	940	1	53.94	1.98	53.94	2.09
		50	53.1	1.96	53.1	2.07
		100	54.47	1.97	54.47	2.01
PMPO film in [EPI ⁺][TFSI ⁻]	584	1	18.02	2.05	18.02	1.76
		50	18.01	2.04	18.03	1.69
		100	16.98	1.92	16.98	1.76
	890	1	43.99	1.85	43.99	2.02
		50	43.45	1.74	43.45	2.13
		100	43.72	1.87	43.87	2.01
PANIL film in [EPI ⁺][TFSI ⁻]	566	1	15.83	2.05	15.82	2.05
		50	15.26	2.06	15.25	2.09
		100	15.09	2.01	15.09	2.08
	950	1	46.17	1.97	46.17	2.10
		50	44.63	1.94	44.63	2.28
		100	39.44	2.08	39.44	2.14
PMPS/PProDOT-Et ₂ ECD	590	1	32.51	1.00	32.51	1.10
		50	30.43	0.94	30.43	1.00
		100	31.92	0.99	31.91	1.01
PMPO/PProDOT-Et ₂ ECD	626	1	41.13	1.54	41.13	1.10
		50	39.43	1.45	39.43	0.98
		100	38.50	1.42	38.50	1.12
PANIL/PProDOT-Et ₂ ECD	628	1	25.00	1.21	25.00	1.06
		50	22.23	1.14	22.23	1.03
		100	21.71	1.17	21.71	1.06

Table 7 Color-bleach kinetics of a PTTTP film and its ECD (Wang and Wu et al. 2020).

Polymers and ECDs	λ_{max}/nm	Cycle No.	T			τ ($T_{90\%}$)		Stability (100 cycles)
			$T_b/\%$	$T_c/\%$	$\Delta T/\%$	τ_c/s	τ_b/s	
PTTTP in [EPI ⁺][TFSI ⁻]	532	1	51.9	41.7	10.2	2.32	1.99	-
		50	49.6	40.7	8.9	2.33	1.86	-
		100	48.7	40.4	8.3	2.29	2.07	81.4%
	1050	1	77.7	53.2	24.5	2.41	1.87	-
		50	76.4	51.9	24.5	2.41	1.89	-
		100	75.3	52.4	22.9	2.39	1.95	93.5%
PTTTP/PProDOT-Et ₂ ECD	588	1	47.9	12.2	35.7	0.96	0.97	-
		50	47.8	12.8	35.0	0.94	0.94	-
		100	48.0	13.9	34.1	0.99	0.92	95.5%

Table 8 Color-bleach kinetics of a PDTPP film and its ECD (Wu and Tung et al. 2018).

Polymer films	λ/nm	Cycle No.	Optical contrast/%			τ/s		Stability (100 cyc)
			$T_b/\%$	$T_c/\%$	$\Delta T/\%$	τ_c/s	τ_b/s	
PDTPP	409	1	47.7	29.6	18.1	1.74	1.60	-
		50	47.2	29.6	17.6	1.46	1.40	-
		100	46.8	29.6	17.2	1.60	1.47	95%
	572	1	52.5	42.4	10.1	2.40	0.85	-
		50	52.3	42.8	9.5	2.40	0.95	-
		100	52.1	42.7	9.4	2.44	0.87	93%
	970	1	75.9	39.2	36.7	1.68	1.77	-
		50	75.2	39.3	35.9	1.60	1.73	-
		100	74.8	39.6	35.2	1.68	1.85	96%
PDTPP/PProDOT-Et ₂	594	1	54.8	11.3	43.5	0.94	0.95	-
		50	54.5	11.2	43.3	0.97	0.97	-
		100	53.8	11.5	42.3	0.99	0.97	97%

Table 9 Color-bleach kinetics of a PFPT film and its ECD (Wang, Chang, and Wu et al. 2019).

Polymer films	λ/nm	Cycle No.	Optical contrast			τ ($T_{90\%}$)		Stability (100cyc)
			$T_b/\%$	$T_c/\%$	$\Delta T/\%$	τ_c/s	τ_b/s	
PFPT	590	1	45.7	39.5	6.2	1.91	1.99	-
		50	43.9	39.5	4.4	1.82	1.95	-
		100	43.9	39.4	4.5	1.82	2.03	72.6%
	1320	1	59.1	36.4	22.7	1.90	1.97	-
		50	58.3	37.3	21.0	1.97	1.91	-
		100	57.6	37.9	19.7	1.90	1.91	86.8%
PFPT/PProDOT-Et ₂	590	1	46.1	12.8	33.3	1.01	0.89	-
		50	46.3	13.2	33.1	0.87	0.87	-
		100	46.8	13.7	33.1	0.93	0.87	99.4%

The optical contrast ($\Delta T\%$) is an important characteristic in electrochromic applications (Ak *et al.* 2016). The ΔT_{\max} of the PMPS, PMPO, PANIL, PTTTP, PDTTTP, and PFTP films are 18.62%, 18.02%, 15.83%, 10.2%, 10.1%, and 6.2% at 600 nm, 584 nm, 566 nm, 532 nm, 572 nm, and 590 nm respectively, in the ionic solution. Moreover, the ΔT_{\max} of the PMPS, PMPO, PANIL, PTTTP, PDTTTP, and PFTP films are 54.47%, 43.99%, 46.17%, 24.5%, 36.7%, and 22.7% at 940 nm, 890 nm, 950 nm, 1050 nm, 970 nm, and 1320 nm respectively, in the ionic solution. The PMPS film shows the highest ΔT_{\max} (54.47% at 940 nm) among these polymer films. The coloration efficiency (CE) is also a useful parameter in electrochromic applications. CE can be calculated using the following equations at a specific wavelength (Chang and Wu *et al.* 2014):

$$\Delta OD = \log(T_b/T_c) \quad (4)$$

$$\eta = \Delta OD/Q_d \quad (5)$$

where ΔOD represents the variation of the optical density at a specific wavelength. T_b and T_c denote the transmittance of the bleaching state and coloring state, respectively. CE (η) stands for the power efficiency of the electrochromic materials and devices. Q_d ($\text{mC}\cdot\text{cm}^{-2}$) is the charge density electrodes. The η_{\max} of the PMPS, PMPO, PANIL, PTTTP, PDTTTP, and PFTP films are $298.28 \text{ cm}^2\cdot\text{C}^{-1}$ at 940 nm, $142.48 \text{ cm}^2\cdot\text{C}^{-1}$ at 890 nm, $279.19 \text{ cm}^2\cdot\text{C}^{-1}$ at 950 nm, $379.64 \text{ cm}^2\cdot\text{C}^{-1}$ at 1050 nm, $303.8 \text{ cm}^2\cdot\text{C}^{-1}$ at 970 nm, and $181.8 \text{ cm}^2\cdot\text{C}^{-1}$ at 1320 nm, respectively (Su and Wu *et al.* 2017; Wang and Wu *et al.* 2020; Wu and Tung *et al.* 2018; Wang, Chang, and Wu *et al.* 2019).

Table 10 Comparisons of the ΔT_{\max} and η_{\max} for PMPS, PMPO, and PANIL films and ECDs (Su and Wu *et al.* 2017).

Polymer Films and ECDs	λ/nm	E_g/eV	$\Delta T_{\max}/\%$	$\Delta OD_{\max}/\%$	$\eta_{\max}/\text{cm}^2\cdot\text{C}^{-1}$
PMPS	940	2.17	54.74	46.40	298.28
PMPO	890	2.25	43.87	30.04	142.48
PANIL	950	2.21	44.63	34.94	279.19
PMPS/PProDOT-Et ₂ ECD	590	-	32.51	54.45	637.25
PMPO/PProDOT-Et ₂ ECD	626	-	41.13	52.40	674.67
PANIL/PProDOT-Et ₂ ECD	628	-	25.00	29.80	401.63

Table 11 Comparisons of the ΔT_{\max} and η_{\max} for PTTTP, PDTTTP, and PFTP films and ECDs (Wang and Wu *et al.* 2020; Wu and Tung *et al.* 2018; Wang, Chang, and Wu *et al.* 2019).

Polymers and ECDs	λ/nm	E_g/eV	$\Delta T_{\max}/\%$	$\Delta OD_{\max}/\%$	$\eta_{\max}/\text{cm}^2\cdot\text{C}^{-1}$
PTTTP	1050	2.34	24.5	16.5	379.64
PTTTP/PProDOT-Et ₂ ECD	588	-	35.7	59.4	890.96
PDTTTP	970	2.24	36.7	28.7	303.8
PDTTTP/PProDOT-Et ₂ ECD	594	-	43.5	59.7	895.5
PFPT	1320	2.26	22.7	21.1	181.8
PFPT/PProDOT-Et ₂ ECD	590	-	33.3	53.4	533.5

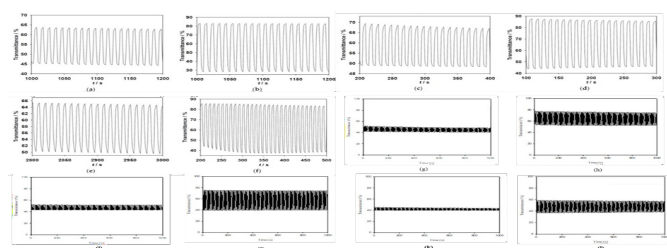


Fig. 7 Transmittance datum of (a) PMPS film at 600 nm; (b)

PMPS film at 940 nm; (c) PMPO film at 584 nm; (d) PMPO film at 950 nm; (e) PANIL film at 566 nm; (f) PANIL film at 950 nm; (g) PTTTP film at 532 nm; (h) PTTTP film at 1050 nm; (i) PDTTTP film at 572 nm; (j) PDTTTP film at 970 nm; (k) PFTP films at 590 nm; and (l) PFTP films at 1320 nm as a function of time in ionic solution. The conducting polymer films were measured with repeated potential between -0.2 and $+0.9$ V every 5 s (Su and Wu *et al.* 2017; Wang and Wu *et al.* 2020; Wu and Tung *et al.* 2018; Wang, Chang, and Wu *et al.* 2019).

3.3 Spectroelectrochemistry of ECDs

Dual-type ECDs composed of two electrochromic electrodes, one anodically coloring layer (PMPS, PMPO, PANIL, PTTTP, PDTTTP, or PFTP) and the other cathodically coloring material (PProDOT-Et₂) were facing each other and were separated by an electrolyte membrane. Figure 8a shows the spectroelectrochemical spectra of the PMPS/PProDOT-Et₂ ECD at potentials between -0.4 V and $+1.6$ V. PMPS/PProDOT-Et₂ ECD shows a peak at around 380 nm and a shoulder at around 430 nm at 0 V, and this can be attributed to the $\pi-\pi^*$ transition peak of the PMPS film in the neutral state. In this situation, PProDOT-Et₂ light blue in its oxidation state, and the PMPS/PProDOT-Et₂ ECD was greyish-green at 0 V. However, the absorption of the $\pi-\pi^*$ transition peak for the PMPS film lessened and a new peak at 590 nm emerged at $+1.6$ V, and the PMPS/PProDOT-Et₂ ECD was cyan at $+1.6$ V. Under similar conditions, the PMPO/PProDOT-Et₂ ECD was light green at -0.4 V, bluish-grey at 0.6 V, light blue at 0.8 V, and blue 1.6 V. The PANIL/PProDOT-Et₂ ECD was grey at -0.4 V, light blue at 0.8 V, and blue at 1.6 V. As presented in Figure 8f, PTTTP/PProDOT-Et₂ ECD displayed an absorption peak at ca. 367 nm at -0.4 V, which could be ascribed to the $\pi-\pi^*$ transition of PTTTP in the reduced state. Under the situation, the cathodic layer was light blue in its oxidized state, and PTTTP/PProDOT-Et₂ ECD was gray at -0.4 V. However, the $\pi-\pi^*$ transition peak of PTTTP decreased gradually and a peak emerged at 588 nm progressively with increasing voltage. The PTTTP/PProDOT-Et₂ ECD was deep blue at 1.2 V. Figs. 8g display the spectroelectrochemical spectra of the PDTTTP/PProDOT-Et₂ ECD at various applied potential. At -0.4 V, the PDTTTP/PProDOT-Et₂ ECD displayed distinct absorption bands at ca. 439 nm, which was in keeping with the $\pi-\pi^*$ transition of the film in reduced states. In such a situation, the cathodic PProDOT-Et₂ film was in an oxidized state and revealed no significant spectral characteristics in the visible spectral region. An increase in the applied potential resulted in oxidation of the PDTTTP, film and reduction of the cathodic PProDOT-Et₂ film, resulting in a new absorption band emerging at 592–594 nm. Furthermore, the predominant color of the PDTTTP/PProDOT-Et₂ ECD was blue at a potential larger than $+1.2$ V. PFPT/PProDOT-Et₂ presented precise absorption shoulders or peaks at ca. 407 nm at 0 V, respectively, which was in agreement with the $\pi-\pi^*$ transition of the PFPT film in neutral states. In the circumstance, the PProDOT-Et₂ layer was classified as in an oxidized state and presented no conspicuous characteristic peak in the UV–Vis zone (Wu *et al.* 2017). An increase of applied voltage resulted in the oxidation of anodically coloring layers and the reduction of the cathodically coloring layers. Accordingly, absorption peaks of ECDs started to appear at 586–612 nm, the pre-eminent color of three ECDs was dark blue at a voltage $\geq +1.2$ V (Su and Wu *et al.* 2017; Wang and Wu *et al.* 2020; Wu and Tung *et al.* 2018; Wang, Chang, and Wu *et al.* 2019).

The CIE chromaticity values (x , y) and colorimetric values (L , a , b , L^* , a^* , b^*) of the PMPS/PProDOT-Et₂, PMPO/PPro-

DOT-Et₂, and PANIL/PProDOT-Et₂ dual type ECDs are summarized in Table 12. Table 13 shows the CIE chromaticity values (x, y) and colorimetric values (L, a, b, L*, a*, b*) of the PTTTPP/PProDOT-Et₂, PDTTTPP/PProDOT-Et₂, and PFTTPP/PProDOT-Et₂ dual type ECDs. Moreover, the CIE chromaticity diagrams of the PMPS/PProDOT-Et₂ ECD at -0.6 and 1.6 V, PMPO/PProDOT-Et₂ and PANIL/PProDOT-Et₂ ECDs at -0.4 and 1.8 V, PTTTPP/PProDOT-Et₂, PDTTTPP/PProDOT-Et₂, and PFTTPP/PProDOT-Et₂ ECDs at -0.4 and 1.2 V are displayed in Figure 9a-f (Su and Wu et al. 2017; Wang and Wu et al. 2020; Wu and Tung et al. 2018; Wang, Chang, and Wu et al. 2019).

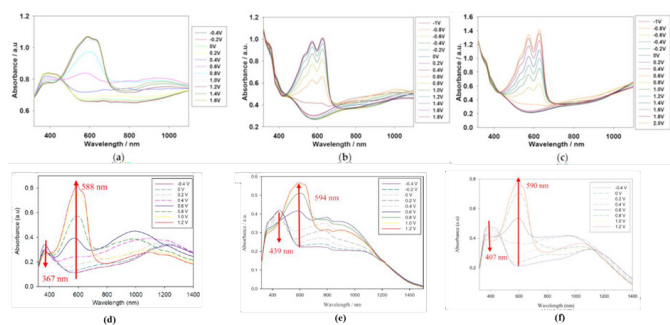


Fig. 8 Spectroelectrochemical spectra of (a) PMPS/PProDOT-Et₂, (b) PMPO/PProDOT - Et₂, (c) PANIL/PProDOT-Et₂, (d) PTTTPP/PProDOT-Et₂, (e) DTTTPP/PProDOT-Et₂, and (f) PFTTPP/PProDOT-Et₂ ECDs at various potentials from -0.4 to 2.0 eV (Su and Wu et al. 2017; Wang and Wu et al. 2020; Wu and Tung et al. 2018; Wang, Chang, and Wu et al. 2019).

Table 12 The colorimetric values (L, a, b, L*, a*, b*) and CIE chromaticity values (x, y) of PMPS/PProDOT-Et₂, PMPO/PProDOT-Et₂, and PANIL/PProDOT-Et₂ ECDs at different applied potentials (Su and Wu et al. 2017).

ECDs	E/V	L	a	b	L*	a*	b*	x	y
PMPS/PProDOT-Et ₂	-0.6	78.12	-1.07	11.74	82.39	-0.02	12.28	0.3354	0.3449
	-0.4	78.13	-1.13	11.79	82.4	-0.08	12.33	0.3355	0.345
	-0.2	78.13	-1.27	11.77	82.4	-0.23	12.31	0.3352	0.3451
	0	78	-1.67	11.35	82.3	-0.65	11.8	0.3335	0.3444
	0.2	77.44	-2.18	10.21	81.82	-1.19	10.48	0.33	0.3421
	0.4	75.55	-1.87	7.83	80.22	-0.9	7.77	0.3252	0.3364
	0.6	69.94	0.1	1.09	75.4	1.13	0.32	0.3129	0.3189
	0.8	64.41	-0.34	-6.29	70.52	0.58	-7.49	0.2942	0.3009
PMPO/PProDOT-Et ₂	1.0	61.4	0.1	-10.71	67.8	1.05	-11.97	0.2839	0.2893
	1.2	60.73	0.72	-12.22	67.18	1.73	-13.46	0.2814	0.2851
	1.4	60.42	1.34	-13.27	66.91	2.43	-14.47	0.2801	0.2822
	1.6	60.06	1.91	-13.56	66.57	3.07	-14.76	0.2804	0.2809
	-0.4	69.99	-1.97	16.09	75.44	-1.11	18.83	0.3498	0.3626
	-0.2	69.92	-2.32	15.75	75.38	-1.49	18.37	0.3482	0.362
	0	69.45	-2.75	14.84	74.97	-1.97	17.17	0.3449	0.3599
	0.2	67.75	-2.44	12.62	73.48	-1.68	14.35	0.3397	0.3538
PANIL/PProDOT-Et ₂	0.4	61.31	-1.16	5.04	67.72	-0.38	5.12	0.322	0.332
	0.6	51.91	-1.54	-7.26	58.93	-1	-8.84	0.2851	0.2958
	0.8	46.45	-0.32	-14.88	53.58	0.38	-16.8	0.2641	0.2704
	1.0	42.8	1.68	-19.68	49.88	2.84	-21.55	0.2532	0.2526
	1.2	40.43	3.4	-22.6	47.43	5.03	-24.36	0.2476	0.2409
	1.4	38.94	4.52	-24.8	45.86	6.47	-26.39	0.2431	0.2326
	1.6	38.48	4.79	-25.17	45.37	6.82	-26.75	0.2423	0.2307
	1.8	38.23	5.13	-25.7	45.1	7.26	-27.22	0.2415	0.2288
PANTIL/PProDOT-Et ₂	-0.4	74.98	-4.17	19.46	79.74	-3.36	22.84	0.3526	0.3715
	-0.2	75	-4.33	19.37	79.75	-3.53	22.71	0.352	0.3713
	0	74.85	-4.6	19.02	79.63	-3.83	22.24	0.3506	0.3706
	0.2	74.5	-4.9	18.3	79.33	-4.16	21.27	0.3482	0.369
	0.4	73.33	-4.61	17.25	78.33	-3.89	19.97	0.3463	0.3664
	0.6	66.93	-2.76	11.09	72.76	-2.05	12.41	0.3349	0.3498
	0.8	55.45	-4.98	-2.59	62.29	-5.02	-3.69	0.2916	0.3135
	1.0	48.59	-4.69	-11.81	55.7	-5.01	-13.66	0.2634	0.2843
	1.2	44.1	-2.96	-18.32	51.2	-3.01	-20.21	0.2465	0.2615
	1.4	40.04	-0.32	-24.33	47.01	0.28	-25.89	0.2334	0.2392
1.6	35.72	3.14	-30.97	42.4	4.81	-31.75	0.2204	0.214	
1.8	32.91	5.48	-35.32	39.29	7.97	-35.34	0.212	0.1975	

Table 13 Photoimages and L*, a*, and b* values of PTTTPP, PDTTTPP, and PFTTP ECDs (Wang and Wu et al. 2020; Wu and Tung et al. 2018; Wang, Chang, and Wu et al. 2019).

ECDs	E/V	Photoimages	L*	a*	b*
PTTTPP/PProDOT-Et ₂	-0.4		87.38	-1.64	8.91
	0		85.98	-2.28	5.47
	0.6		72.62	4.5	-10.44
	0.8		65.31	4.11	-19.6
	1.2		56.03	5.65	-30.98
PDTTTPP/PProDOT-Et ₂	-0.4		75.88	3.83	19.11
	-0.2		75.89	3.29	18.74
	0.2		75.20	0.07	13.81
	0.4		72.08	0.98	7.22
	0.6		66.16	1.29	-3.30
	0.8		60.27	0.71	-13.27
	1.0		57.91	1.53	-17.60
1.2		57.50	2.25	-19.01	
PFTTPP/PProDOT-Et ₂	-0.4		78.4	0.2	17.82
	0.6		64.26	1.02	-8.07
	0.8		58.56	1.63	-16.23
	1.2		55.7	3.59	-20.22

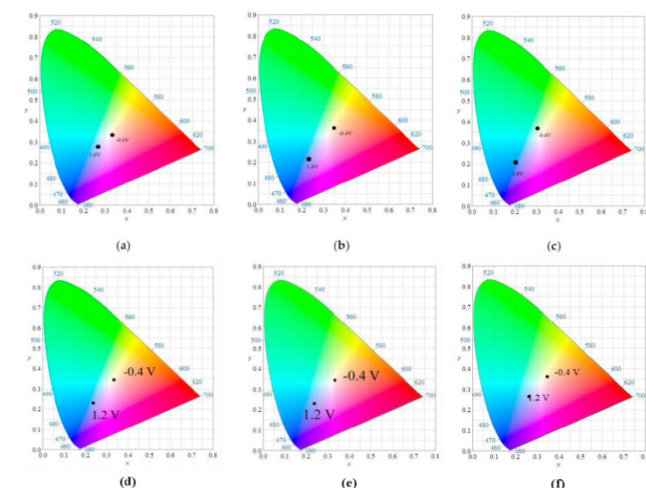


Fig. 9 CIE chromaticity diagrams of (a) PMPS/PProDOT-Et₂ at -0.6 V (neutral) and 1.6 V (oxidation); (b) PMPO/PProDOT-Et₂ at -0.4 V (neutral) and 1.8 V (oxidation); (c) PANIL/PProDOT-Et₂ at -0.4 V (neutral) and 1.8 V (oxidation); (d) PTTTPP/PProDOT-Et₂ at -0.4 V (neutral) and 1.2 V (oxidation); (e) PDTTTPP/PProDOT-Et₂ at -0.4 V (neutral) and 1.2 V (oxidation); and (f) PFTTPP/PProDOT-Et₂ at -0.4 V (neutral) and 1.2 V (oxidation) (Su and Wu et al. 2017; Wang and Wu et al. 2020; Wu and Tung et al. 2018; Wang, Chang, and Wu et al. 2019).

The transmittance-time profiles of the PMPS/PProDOT-Et₂, PMPO/PProDOT-Et₂, PANIL/PProDOT-Et₂, PTTTPP/PProDOT-Et₂, PDTTTPP/PProDOT-Et₂, and PFTTPP/PProDOT-Et₂ ECDs are shown in Figure 10. The ΔT_{max}% of the PMPS/PProDOT-Et₂, PMPO/PProDOT-Et₂, PANIL/PProDOT-Et₂, PTTTPP/PProDOT-Et₂, PDTTTPP/PProDOT-Et₂, and PFTTPP/PProDOT-Et₂ ECDs were 33% at 590 nm, 41% at 626 nm, 25% at 628 nm,

35.7% at 588 nm, 43.5% at 594 nm, 33.3% at 590 nm, respectively. The η of the PMPS/PProDOT-Et₂, PMPO/PProDOT-Et₂, PANIL/PProDOT-Et₂, PTTTP/PProDOT-Et₂, PDTPP/PProDOT-Et₂, and PFPT/PProDOT-Et₂ ECDs calculated from Equations (1) and (2), were found to be 637.25 cm² · C⁻¹ at 590 nm, 674.67 cm² · C⁻¹ at 626 nm, 401.63 cm² · C⁻¹ at 628 nm, 890.96 cm² · C⁻¹ at 588 nm, 895.5 cm² · C⁻¹ at 594 nm, and 533.5 cm² · C⁻¹ at 590 nm, respectively. The PTTTP/PProDOT-Et₂ and PDTPP/PProDOT-Et₂ ECDs showed higher ΔT_{\max} and η than those ECDs, indicating that the incorporations of the trifluoromethoxy-phenyl- and thio-phenyl- phenyl- substituted PSNs into the ECDs gave rise to higher ΔT_{\max} and η than those of others substituted PSNs (Su and Wu et al. 2017; Wang and Wu et al. 2020; Wu and Tung et al. 2018; Wang, Chang, and Wu et al. 2019).

The ΔT_{\max} , ΔOD , and η_{\max} of the PMPS/PProDOT-Et₂, PMPO/PProDOT-Et₂, PANIL/PProDOT-Et₂, PTTTP/PProDOT-Et₂, PDTPP/PProDOT-Et₂, and PFPT/PProDOT-Et₂ ECDs are summarized in Table 10 and Table 11. The τ_c and τ_b estimated at various double-step potential cycles are listed in Table 6, Table 7, Table 8, and Table 9. The $T_{95\%}$ of the PMPS/PProDOT-Et₂ ECD at 590 nm was estimated to be 0.99 s from the bleaching state to the coloring state and 1.01 s from the coloring state to the bleaching state at the 100th cycle. Under similar conditions, the $T_{95\%}$ of the PMPO/PProDOT-Et₂ ECD at 626 nm was estimated to be 1.42 s from the bleaching state to the coloring state and 1.12 s from the coloring state to the bleaching state at the 100th cycle, and the $T_{95\%}$ of the PANIL/PProDOT-Et₂ ECD at 628 nm was estimated to be 1.17 s from the bleaching state to the coloring state and 1.06 s from the coloring state to the bleaching state. Moreover, the $T_{95\%}$ of the PTTTP/PProDOT-Et₂ ECD at 588 nm was estimated to be 0.99 s from the bleaching state to the coloring state and 0.92 s from the coloring state to the bleaching state. The $T_{95\%}$ of the PDTPP/PProDOT-Et₂ ECD at 594 nm was estimated to be 0.99 s from the bleaching state to the coloring state and 0.97 s from the coloring state to the bleaching state. The $T_{95\%}$ of the PFPT/PProDOT-Et₂ ECD at 590 nm was estimated to be 0.93 s from the bleaching state to the coloring state and 0.87 s from the coloring state to the bleaching state. The PMPS/PProDOT-Et₂, PDTPP/PProDOT-Et₂, and PFPT/PProDOT-Et₂ ECDs presented shorter τ_c and τ_b than those of the PMPO/PProDOT-Et₂ and PANIL/PProDOT-Et₂ ECDs at the 100th cycle, implying that the PMPS/PProDOT-Et₂, PDTPP/PProDOT-Et₂, and PFPT/PProDOT-Et₂ ECDs changed color faster from the bleaching state to the coloring state than those of the PMPO/PProDOT-Et₂ and PANIL/PProDOT-Et₂ ECDs (Su and Wu et al. 2017; Wang and Wu et al. 2020; Wu and Tung et al. 2018; Wang, Chang, and Wu et al. 2019).

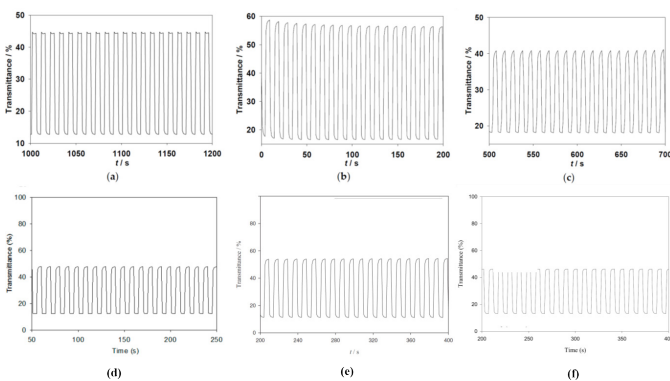


Fig. 10 Transmittance-time profiles of (a) PMPS/PProDOT-Et₂ ECD at 590 nm as a function of time, the ECD was stepped by repeated potential between -0.4 and $+1.0$

V; (b) PMPO/PProDOT-Et₂ ECD at 626 nm, the ECD was stepped by repeated potential between -0.4 and 1.2 V; (c) PANIL/PProDOT-Et₂ ECDs at 628 nm, the ECD was stepped by repeated potential between 0 and 1.2 V; (d) PTTTP/PProDOT-Et₂ ECD at 588 nm as a function of time, the ECD was stepped by repeated potential between -0.2 and $+1.0$ V; (e) PDTPP/PProDOT-Et₂ ECD at 594 nm as a function of time, the ECD was stepped by repeated potential between -0.8 and $+1.4$ V; and (f) PFPT/PProDOT-Et₂ ECD at 590 nm as a function of time, the ECD was stepped by repeated potential between -0.2 and $+1.2$ V (Su and Wu et al. 2017; Wang and Wu et al. 2020; Wu and Tung et al. 2018; Wang, Chang, and Wu et al. 2019).

The long-term switching stability of the ECDs between the bleaching and coloring states is an important parameter in practical applications of ECDs (Wu and Su et al. 2015; Gültekin et al. 2012). The cycling stability of the PMPS/PProDOT-Et₂, PMPO/PProDOT-Et₂, and PANIL/PProDOT-Et₂ ECDs were measured using CV at potentials between -0.4 and $+1.4$ V with a scan rate of $100 \text{ mV} \cdot \text{s}^{-1}$, however, under the similar condition of the PTTTP/PProDOT-Et₂, PDTPP/PProDOT-Et₂, and PFPT/PProDOT-Et₂ ECDs were monitored by CV at voltages between -1.0 and $+1.8$ V. As shown in Figure 11, 94%, 91%, 90%, 95.2%, 94.7%, and 93.7% of the electrical activity was retained after 500 cycles for the PMPS/PProDOT-Et₂, PMPO/PProDOT-Et₂, PANIL/PProDOT-Et₂, PTTTP/PProDOT-Et₂, PDTPP/PProDOT-Et₂, and PFPT/PProDOT-Et₂ ECDs, respectively, and 91%, 89%, 87%, 88.9%, 94.7%, and 90.9% of the electrical activity was retained after 1000 cycles for the PMPS/PProDOT-Et₂, PMPO/PProDOT-Et₂, and PANIL/PProDOT-Et₂ ECDs, respectively, indicating that the PMPS/PProDOT-Et₂, PMPO/PProDOT-Et₂, PANIL/PProDOT-Et₂, PTTTP/PProDOT-Et₂, PDTPP/PProDOT-Et₂, and PFPT/PProDOT-Et₂ ECDs displayed reasonable long-term cycling stability (Su and Wu et al. 2017; Wang and Wu et al. 2020; Wu and Tung et al. 2018; Wang, Chang, and Wu et al. 2019).

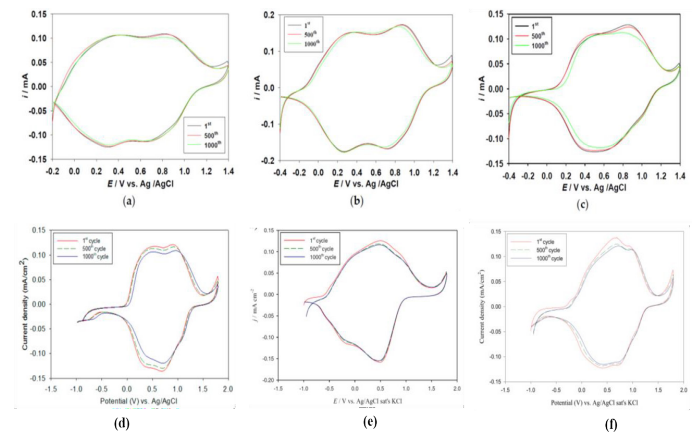


Fig. 11 Cyclic voltammograms of (a) PMPS/PProDOT-Et₂; (b) PMPO/PProDOT-Et₂; (c) PANIL/PProDOT-Et₂; (d) PTTTP/PProDOT-Et₂; (e) PDTPP/PProDOT-Et₂, and (f) PFPT/PProDOT-Et₂ ECDs as a function of repeated scans at $100 \text{ mV} \cdot \text{s}^{-1}$ (Su and Wu et al. 2017; Wang and Wu et al. 2020; Wu and Tung et al. 2018; Wang, Chang, and Wu et al. 2019).

The optical memory effect is also important for ECD applications (Wu and Chung et al. 2016). The optical memory of the

PMPS/PProDOT-Et₂, PMPO/PProDOT-Et₂, PANIL/PProDOT-Et₂, PTTTP/PProDOT-Et₂, PDTTPP/PProDOT-Et₂, and PFPT/PProDOT-Et₂ ECDs was evaluated at 590, 626, 628, 588, 594, and 590 nm, respectively, with the function of time at -0.4 V and +1.0 V by applying a potential for 1 s for each 200 s time interval. As shown in Figure 12a-f, the PMPS/PProDOT-Et₂, PMPO/PProDOT-Et₂, PANIL/PProDOT-Et₂, PTTTP/PProDOT-Et₂, PDTTPP/PProDOT-Et₂, and PFPT/PProDOT-Et₂ ECDs showed good optical memories in a reduced state of the PMPS, PMPO, PANIL, PTTTP, PDTTPP, and PFPT films, and the transmittance change of the PMPS, PMPO, PANIL, PTTTP, PDTTPP, and PFPT films is less than 1% in their reduced states. However, in the oxidized state of the PMPS, PMPO, PANIL, PTTTP, PDTTPP, and PFPT films and in the reduced state of the PProDOT-Et₂ film, the PMPS/PProDOT-Et₂, PMPO/PProDOT-Et₂, PANIL/PProDOT-Et₂, PTTTP/PProDOT-Et₂, PDTTPP/PProDOT-Et₂, and PFPT/PProDOT-Et₂ ECDs are less stable than the oxidized state of the PProDOT-Et₂ film, but the transmittance change is less than 3% in the oxidized state of the PMPS, PMPO, PANIL, PTTTP, PDTTPP, and PFPT films, demonstrating that the PMPS/PProDOT-Et₂, PMPO/PProDOT-Et₂, PANIL/PProDOT-Et₂, PTTTP/PProDOT-Et₂, PDTTPP/PProDOT-Et₂, and PFPT/PProDOT-Et₂ ECDs show reasonable optical memory in the coloring and bleaching states (Su and Wu et al. 2017; Wang and Wu et al. 2020; Wu and Tung et al. 2018; Wang, Chang, and Wu et al. 2019).

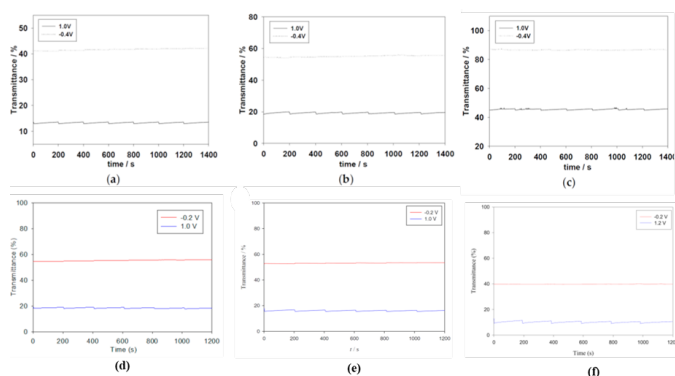


Fig. 12 Open circuit stability of (a) PMPS/PProDOT-Et₂ ECD monitored at 590 nm; (b) PMPO/PProDOT-Et₂ ECD monitored at 626 nm; (c) PANIL/PProDOT-Et₂ ECD monitored at 628 nm; (d) PTTTP/PProDOT-Et₂ ECD monitored at 588 nm; (e) PDTTPP/PProDOT-Et₂ ECD monitored at 594 nm, and (f) PFPT/PProDOT-Et₂ ECD monitored at 590 nm (Su and Wu et al. 2017; Wang and Wu et al. 2020; Wu and Tung et al. 2018; Wang, Chang, and Wu et al. 2019).

4. CONCLUSION

The dithienylpyrrole derivative was synthesized via a Knorr-Paal reaction and its corresponding homopolymer was prepared by using electrochemical polymerization. According to the spectroelectrochemical analysis, the PMPS, PMPO, PANIL, PTTTP, PDTTPP, and PFPT films revealed distinct electrochromic properties at various potentials in an ionic liquid solution. The PTTTP film showed the highest coloration efficiency than those of the PDTTPP, PMPS, PMPO, PANIL and PFPT films. Dual-type complementary ECDs consisting of PMPS, PMPO, PANIL, PTTTP, PDTTPP, and PFPT films as anodically coloring materials and

PProDOT-Et₂ as the cathodically coloring material was fabricated. Spectroelectrochemical studies showed that the PMPS/PProDOT-Et₂ ECD is greyish-green and cyan at 0 and +1.6 V, respectively. Electrochromic switching studies showed that the PMPS/PProDOT-Et₂ ECD exhibited high ΔT_{\max} (32.51%) and coloration efficiency (637.25 cm² · C⁻¹) at 590 nm. Considering these results, PMPS film is a promising anodic layer for electrochromic applications. The anodic polymer films display reversible electrochromic phenomena in their neutral and oxidized states.

However, the PTTTP film was grayish-yellow at 0 V, grayish-blue at 1.0 V, and bluish-violet at 1.4 V. Colorless-to-colorful switching investigations of anodic films show that PTTTP film has high η (379.64 cm²/C at 1050 nm), whereas PTTTP/PProDOT-Et₂ ECD displays high η (890.96 cm²/C at 588 nm) and adequate optical memory at coloring and bleaching states, implying PTTTP films are promising candidates as anodic electrochromic materials for potential applications in motorcycle helmet-visors, electrochromic goggles, electrochromic display devices, and PFPT/PProDOT-Et₂ ECD realized high ΔT_{\max} (33.3%), ΔOD_{\max} (53.4%) and η (533.5 cm² C⁻¹). A dual type PDTTPP/PProDOT-Et₂ ECD revealed yellowish green and dark blue coloration at -0.2 V and 1.2 V, respectively, and attained a high ΔT_{\max} (43.5%, at 594 nm) and short switching time (less than 1 s). PFPT/PProDOT-Et₂ ECD realized high ΔT_{\max} (33.3%), ΔOD_{\max} (53.4%) and η (533.5 cm² C⁻¹).

Therefore, the application of organic conducting polymers is suitable for electrochromic materials owing to great design flexibility and facile fine-tune their chemical configurations for a wide range of electrochemical and optical properties.

REFERENCES

- Akbaşoğlu, N., Balan, A., Baran, D., Cirpan, A., and Toppare, L. (2010). "Electrochemical and optical studies of furan and thien- o[3,2-b]thiophene end capped benzotriazole derivatives." *Journal of Polymer Science Part A: Polymer Chemistry*, **48**, 5603-5610.
- Amb, C.M., Dyer, A. L., and Reynolds, J. R. (2011). "Navigating the color palette of solution- processable electrochromic polymers." *Chemistry of Materials*, **23**, 397-415.
- Apetrei, R. M. and Camurlu, P. (2020). "Review—functional platforms for (bio)sensing: thiophene-pyrrole hybrid polymers." *Journal of The Electrochemical Society*, **167**, 307557.
- Arslan, A., Türkarslan, Ö., Tanyeli, C., Akhmedov, I. M., and Toppare, L. (2007). "Electrochromic properties of a soluble conducting polymer: poly(1-(4-fluorophenyl)-2,5-di(thiophen-2-yl)-1H-pyrrole)." *Materials Chemistry and Physics*, **104**, 410-416.
- Camurlu, P. and Gültekin, C. (2012). "A comprehensive study on utilization of N-substituted poly(2,5-dithienylpyrrole) derivatives in electrochromic devices." *Solar Energy Materials and Solar Cells*, **107**, 142-147.
- Chang, K. H., Wang, H. P., Wu, T. Y., and Sun, I. W. (2014). "Optical and electrochromic characterizations of four 2,5-dithienylpyrrole-based conducting polymer films." *Electrochimica Acta*, **119**, 225-235.
- Eken, S., Carbas, B. B., Akdağ, A., and Önal, A. M. (2014). "Synthesis of new thienylene pyrrole monomers and their electropolymerizations." *Journal of The Electrochemical Society*, **161**,

- G115-G121.
- Ferraris, J. P., Andrus, R. G., and Hrcir, D. C. (1989). "Steric effects on the optical and electrochemical properties of N-substituted pyrrole-thiophene monomers and polymers." *Journal of the Chemical Society, Chemical Communications*, 1318-1320.
- Gaupp, C. L., Welsh, D. M., and Reynolds, J. R. (2002). "Poly(ProDOT-Et₂): A high-contrast, high-coloration efficiency electrochromic polymer." *Macromolecular Rapid Communications*, **23**, 885-889.
- Huang, J. H., Hsu, C. Y., Hu, C. W., Chu, C. W., and Ho, K. C. (2010). "The influence of charge trapping on the electrochromic performance of poly(3,4-alkylenedioxythiophene) derivatives." *ACS Applied Materials & Interfaces*, **2**, 351-359.
- İçli-Özkut, M. J., Mersini, A., Önal, M., and Cihaner, A. (2012). "Substituent and heteroatom effects on the electrochromic properties of similar systems." *Journal of Polymer Science Part A: Polymer Chemistry*, **50**, 615-621.
- Kim, Y. H., Hwang, J., Son, J. I., and Shim, Y. B. (2010). "Synthesis, electrochemical, and spectroelectrochemical properties of conductive poly-[2,5-di-(2-thienyl)-1H-pyrrole-1- (p-benzoic acid)]." *Synthetic Metals*, **160**, 413-418.
- Kim, Y. H., Hwang, J., Son, J. I., and Shim, Y. B. (2010). "Synthesis, electrochemical, and spectroelectrochemical properties of conductive poly-[2,5-di-(2-thienyl)-1H-pyrrole-1- (p-benzoic acid)]." *Synthetic Metals*, **160**, 413-418.
- Krishnamoorthy, K., Ambade, A. V., Kanungo, M., Contractor, A., and Kumar, A. (2001). "Rational design of an electrochromic polymer with high contrast in the visible region: dibenzyl substituted poly(3,4-propylenedioxythiophene)." *Journal of Materials Chemistry*, **11**, 2909-2911.
- Kuo, C. W., Wu T. Y., and Huang, M. W. (2016). "Electrochromic characterizations of copolymers based on 4,4'-bis(N -carbazolyl)-1,1'-biphenyl and indole-6-carboxylic acid and their applications in electrochromic devices." *Journal of the Taiwan Institute of Chemical Engineers*, **68**, 481-488.
- Kuo, C. W., Wu, T. L., Lin, Y. C., Chang, J. K., Chen, H. R., and Wu, T. Y. (2016). "Copolymers based on 1,3-bis(carbazol-9-yl)benzene and three 3,4-ethylenedioxy thiophene derivatives as potential anodically coloring copolymers in high-contrast electrochromic devices." *Polymers*, **8**, 368.
- Rai, V., Singh, R. S., Blackwood, D. J., and Zhili, D. (2020). "A review on recent advances in electrochromic devices: a material approach." *Advanced Engineering Materials*, **2000082**, 1-23.
- Sim, L. N., Majid, S. R., and Arof, A. K. (2012). "Characteristics of PEMA/PVdF-HFP blend polymeric gel films incorporated with lithium triflate salt in electrochromic device." *Solid State Ionics*, **209-210**, 15-23.
- Soyleyici, S., Karakus, M., and Ak, M. (2016). "Transparent-blue colored dual type electrochromic device: Switchable glass application of conducting organic-inorganic hybrid carbazole polymer." *Journal of the Electrochemical Society*, **163**, H679-H683.
- Su, Y. S., Chang, J. C., and Wu, T. Y. (2017). "Applications of three dithienylpyrroles-based electrochromic polymers in high-contrast electrochromic devices." *Polymers*, **74**, 114-131.
- Tarkuc, S., Sahmetlioglu, E., Tanyeli, C., Akhmedov, I. M., and L. Toppare (2006). "A soluble conducting polymer: 1-phenyl-2,5-di(2-thienyl)-1H-pyrrole and its electrochromic application." *Electrochimica Acta*, **51**, 5412-5419.
- Tsao, M. H., Wu, T. Y., Wang, H. P., Sun, I. W., Su, S. G., Lin, Y. C., and Chang, C. W. (2011). "An efficient metal free sensitizer for dye-sensitized solar cells." *Materials Letters*, **65**, 583-586.
- Wang, W. H., Chang, J. C., Lee, P. Y., Lin, Y. C., and Wu, T. Y. (2020). "4-(Trifluoromethoxy) phenyl-containing polymers as promising anodic materials for electrochromic devices." *Coatings*, **10**, 1251.
- Wang, W. H., Chang, J. C., and Wu, T. Y. (2019). "4-(Furan-2-yl)phenyl-containing polydithienylpyrroles as promising electrodes for high contrast and coloration efficiency electrochromic devices." *Organic Electronics*, **74**, 23-32.
- Wu, T. Y. and Tung, Y. H. (2018). "Phenylthiophene-containing poly(2,5-dithienylpyrrole)s as potential anodic layers for high-contrast electrochromic devices." *Journal of The Electrochemical Society*, **165**, H183-H195.
- Wu, T. Y., and Chung, H. H. (2016). "Applications of tris(4-(thiophen-2-yl)phenyl)amine- and dithienylpyrrole-based conjugated copolymers in high-contrast electrochromic devices." *Polymers*, **8**, 206.
- Wu, T. Y. and Chen, Y. (2002). "Synthesis and characterization of luminescent copolymers containing iminodibenzyl and divinylbenzene chromophores." *Journal of Polymer Science Part A Polymer Chemistry*, **40**, 3847-3857.
- Wu, T. Y. and Su, Y. S. (2015). "Electrochemical synthesis and characterization of a 1,4- benzodioxan-based electrochromic polymer and its application in electrochromic devices." *Journal of the Electrochemical Society*, **162**, G103-G112.
- Yigitsoy, B., Varis, S., Tanyeli, C., Akhmedov, I. M., and Toppare, L. (2007). "A soluble conducting polymer of 2,5-di(thiophen-2-yl)-1-p-tolyl-1H-pyrrole and its electrochromic device." *Thin Solid Films*, **515**, 3898-3904.
- Yildiz, E., Camurlu, P., Tanyeli, C., Akhmedov, I., and Toppare, L. (2007). "A soluble conducting polymer of 4-(2,5-di(thiophen-2-yl)-1H-pyrrol-1-yl)benzenamine and its multichromic copolymer with EDOT." *Journal of Electroanalytical Chemistry*, **612**, 247- 256.
- Yigitsoy, B., Varis, S., Tanyeli, C., Akhmedov, I. M., and Toppare, L. (2007). "Electrochromic properties of a novel low band gap conductive copolymer." *Electrochimica Acta*, **52**, 6561- 6568.
- Yildiz, E., Camurlu, P., Tanyeli, C., Akhmedov, I., and Toppare, L. (2008). "A soluble conducting polymer of 4-(2,5-di(thiophen-2-yl)-1H-pyrrol-1-yl)benzenamine and its multichromic copolymer with EDOT." *Journal of Electroanalytical Chemistry*, **612**, 247- 256.
- Yildiz, E., Camurlu, P., Tanyeli, C., Akhmedov, I., and Toppare, L. (2008). "A soluble conducting polymer of 4-(2,5-di(thiophen-2-yl)-1H-pyrrol-1-yl)benzenamine and its multichromic copolymer with EDOT." *Journal of Electroanalytical Chemistry*, **612**, 247- 256.